ACS NANO

www.acsnano.org

ARTICLE

Merging Single-Atom-Dispersed Silver and Carbon Nitride to a Joint Electronic System *via* Copolymerization with Silver Tricyanomethanide

Zupeng Chen,[†] Sergey Pronkin,[‡] Tim-Patrick Fellinger,[†] Kamalakannan Kailasam,[§,¶] Gianvito Vilé,[⊥] Davide Albani,[⊥] Frank Krumeich,[∥] Rowan Leary,[#] Jon Barnard,[#] John Meurig Thomas,[#] Javier Pérez-Ramírez,[⊥] Markus Antonietti,[†] and Dariya Dontsova*[,†]

[†]Department of Colloid Chemistry, Max-Planck Institute of Colloids and Interfaces, Research Campus Golm, 14424 Potsdam, Germany

[‡]Institut de Chimie et des Procédés pour l'Energie, l'Environnement et la Santé (ICPEES), ECPM, CNRS-Université de Strasbourg (UdS) UMR 7515, 25, rue Becquerel, 67087 Strasbourg, France

[§]Institut für Chemie, Sekr. TC 2, Technische Universität Berlin, Englische Str. 20, 10587 Berlin, Germany

[⊥]Institute for Chemical and Bioengineering, Department of Chemistry and Applied Biosciences, and [∥]Laboratory of Inorganic Chemistry, ETH Zürich, Vladimir-Prelog-Weg 1, 8093 Zürich, Switzerland

[#]Department of Materials Science and Metallurgy, University of Cambridge, 27 Charles Babbage Road, Cambridge CB3 0FS, United Kingdom

Supporting Information

ABSTRACT: **Herein, we present an approach to create a hybrid between single-atom-dispersed silver and a carbon nitride polymer. Silver tricyanomethanide (AgTCM) is used as a reactive comonomer during templated carbon nitride synthesis to introduce both negative charges and silver atoms/ions to the system. The successful introduction of the extra electron density under the formation of a delocalized joint electronic system is proven by photoluminescence measurements, X-ray photoelectron spectroscopy investigations, and measurements of surface ζ-potential. At the same time, the principal structure of the carbon nitride network is not disturbed, as shown by solid-state nuclear magnetic resonance spectroscopy and electrochemical impedance spectroscopy analysis. The synthesis also results in an improvement of the visible light absorption and the development of higher surface area in the final products. The atom-dispersed AgTCM-doped carbon nitride shows an enhanced performance in the selective hydrogenation of alkynes in comparison with the performance of other conventional Ag-based materials prepared by spray deposition and impregnation−reduction methods, here exemplified with 1-hexyne.**

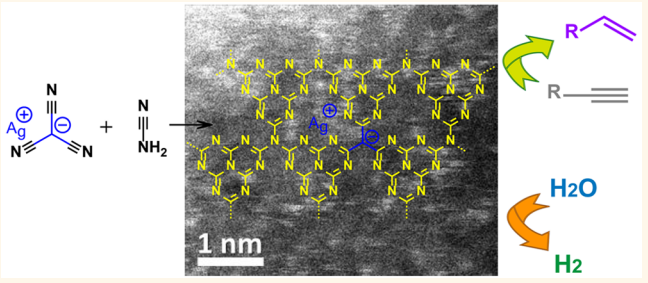

KEYWORDS: *carbon nitride, atomic dispersion, metal doping, copolymerization, joint electronic system, hydrogen evolution, selective hydrogenation*

Carbon nitrides (CN) with a stoichiometry close to C_3N_4 are metal-free organic polymeric semiconductors that have recently attracted remarkable attention as visible light operating photocatalysts for water splitting,[1−3] heterogeneous catalysts for various reactions (*e.g.*, Friedel−Crafts-type reactions, cyclization of functional nitriles[4]), catalyst supports, *etc.* Introduction of different metals into the carbon nitride network was performed in order to improve the light-harvesting ability of the polymer, by analogy with the working principle of metal porphyrins and phthalocyanines.[5] Another goal of metal doping is the preparation of highly active composite systems for various (photo)catalytic applications. Silver was previously introduced in CN polymer composites in

Received: July 8, 2015
Accepted: February 10, 2016
Published: February 10, 2016

DOI: 10.1021/acsnano.5b04210
ACS Nano 2016, 10, 3166−3175

Scheme 1. Expected Modification of the Idealized Carbon Nitride Network Using Silver Tricyanomethanide

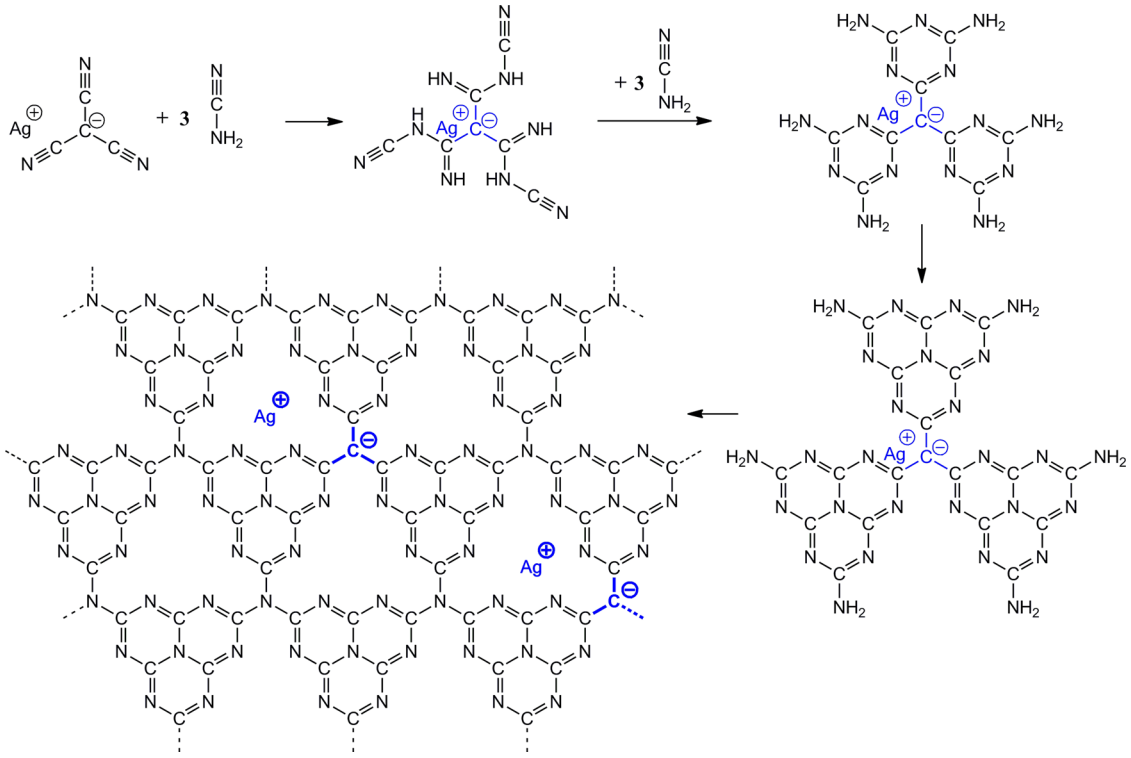

the form of nanoparticles (NPs)[6−12] and as silver compounds being a second semiconductor (*e.g.*, Ag_3PO_4,[13−16] Ag_2O,[17] Ag_2S,[18] AgCl,[19] AgBr[20,21]), and improvements in the performance in photo- or photoelectrocatalytic reactions were reported. Typically, deposition of a metal at carbon nitrides is performed *postsynthetically*, by impregnation of prepared CN polymers with a metal salt, followed by metal reduction and/or heat treatment. This also leads to an undesirable decrease of the total surface area of the final composite compared to original material. Some examples related to the preparation of Ag-containing CN composites illustrating this effect are deposition of Ag_2O on mesoporous graphitic carbon nitride, mpg-CN, which was accompanied by a decrease of the surface area from 336 to 20 m^2/g;[17] during Ag_3PO_4/C_3N_4 composite preparation, the surface area dropped from 23.2 to 0.2 m^2/g;[14] deposition of Ag/AgCl on carbon nitride resulted in a surface area decrease from 9.2 m^2/g to 1.3 m^2/g.[19]

An alternative approach to introduce metals into the C_3N_4 network, potentially even more homogeneous and also into the bulk of the material, comprises the addition of a metal salt *during the synthesis* of carbon nitride.[5] Usually, also in this case, homogeneous metal distribution in the final product is not ensured, as a macroscopic demixing throughout the process might occur. Therefore, it is, in our opinion, crucial to select a suitable miscible and *reactive* metal precursor that would undergo co-condensation with the C_3N_4 precursors in order to ensure homogeneity of the final composite. Metal cyanamides, dicyanamides, and tricyanomethanides are good candidates, but tricyanomethanides present three reactive cyano groups and a flat molecular geometry that potentially favors the incorporation into layered structures typical for CN polymers, as well as it is expected to bring extra electron density, favorable for reductive catalysis.

Catalyzed hydrogenations are fundamental reactions for academics and industry for the preparation of various platform chemicals. Pd-loaded carbon nitrides were reported to have promising catalytic activities for selective hydrogenation of phenols to the corresponding cyclohexanones,[22−24] hydrogenation of quinoline to 1,2,3,4-tretrahydroquinoline,[25] partial hydrogenation of substituted phenylacetylenes to the corresponding styrenes,[26] and many more. Compared to Pd, which is the most efficient known catalyst for this type of reaction,[27] Ag represents a cheaper, less toxic, and less studied alternative. Recently, silver NPs loaded at different inorganic supports were evaluated in the three-phase partial hydrogenation of functionalized alkynes. The catalysts showed remarkable stereo- and chemoselectivity and benefits of low cost and operation at mild reaction conditions.[28]

Herein, we describe a strategy for simultaneous silver doping and introduction of negative charges into the carbon nitride C_3N_4 network by using silver tricyanomethanide (AgTCM) as a reactive comonomer. The introduced negative charges beneficially contribute to the semiconductor structure of carbon nitrides and act as a strong binding site for the atomically distributed silver, promoting charge transport between the metal centers and semiconductor. We exemplify this effect *via* the application of different AgTCM-modified carbon nitrides in the photocatalytic water reduction and three-phase alkyne hydrogenation. It is shown that the catalysts prepared with Ag tricyanomethanide possess indeed improved performance compared to that of conventionally prepared analogous silver materials in nanoparticulate form.

RESULTS AND DISCUSSION

The introduction of both silver ions and negatively charged centers into a C_3N_4 network using silver tricyanomethanide as a comonomer was accomplished using co-condensation with

DOI: 10.1021/acsnano.5b04210
ACS Nano 2016, 10, 3166−3175

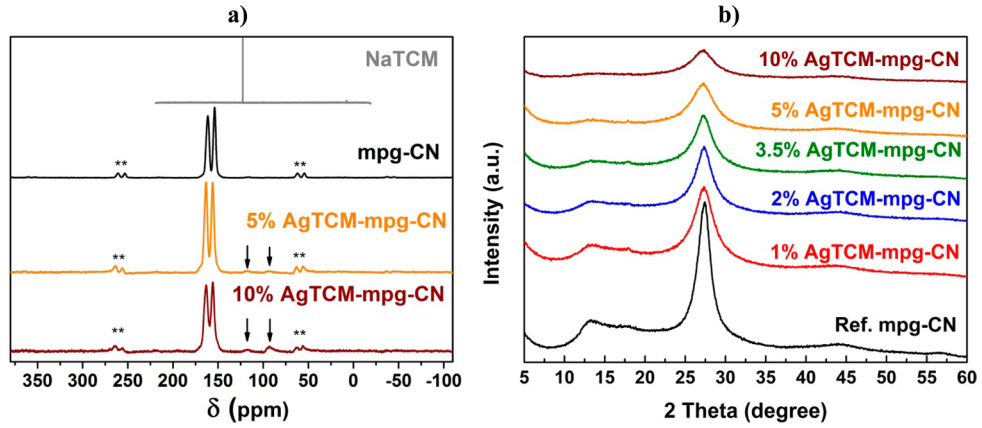

Figure 1. $^{13}C-^{1}H$ CP/MAS NMR spectra of mpg-CN, 5 and 10 wt % AgTCM-mpg-CN, and ^{13}C NMR spectrum of NaTCM in D_2O. Asterisks indicate spinning side bands in the ^{13}C spectra (a). PXRD patterns of the reference mpg-CN and the products prepared using different amounts of AgTCM (b).

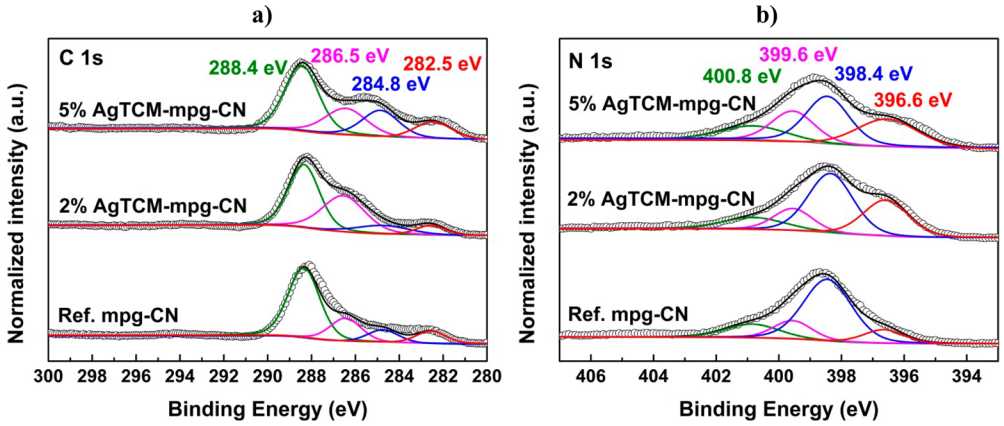

Figure 2. C 1s (a) and N 1s (b) XPS spectra of the reference mpg-CN, 2 and 5 wt % AgTCM-mpg-CN.

cyanamide according to Scheme 1. The behavior of the reaction mixture consisting of AgTCM and cyanamide (using a 1:6 molar ratio, according to the stoichiometry in Scheme 1) was observed by naked eye upon heating in a flask under nitrogen flow. First, cyanamide melts and slowly dissolves the tricyanomethanide to give a transparent yellow solution. After AgTCM is dissolved, a highly exothermic reaction takes place at about 80 °C, and the subsequent reactions proceed in a solid state. However, to avoid an excessive decrease of the useful band gap energy, smaller amounts of the dopant were used in the following synthetic protocols.

In order to develop a high surface area in the final products, which is desirable for most applications, we have used a SiO_2 NP template (details on the synthetic procedure are given in the Materials and Methods section). Different quantities of silver tricyanomethanide, namely, 1, 2, 3.5, 5, and 10 wt % relative to the amount of cyanamide, were applied to successfully introduce the desired amounts of silver into the hybrid structure (Table S1).

The chemical structure of the final AgTCM-doped carbon nitrides is similar to that of the reference mesoporous graphitic carbon nitride (mpg-CN),[29] prepared without dopant, as revealed by the ^{13}C solid-state cross-polarization/magic angle spinning nuclear magnetic resonance (CP/MAS NMR) spectra in Figure 1a. The two main C signals at 163 and 156 ppm in the silver-doped materials are attributed to $CN_2(NH_x)$ and CN_3 moieties, respectively.[30] Upon increase of the AgTCM concentration to 5 or 10 wt %, additional C signals at 117 and 93 ppm assigned to very electron rich, aromatic sp^2-hybridized carbons start to develop, suggesting the successful incorporation of TCM fragments into the final polymer structure. The ^{13}C spectrum of the original tricyanomethanide anion shows mainly the contribution of cyano groups at 123 ppm, while the signal of negatively charged carbon is barely visible at 7.5 ppm.

The introduction of silver ions is accompanied by a slight disturbance of the local C_3N_4 network structure. This is illustrated by the intensity decrease and broadening of the stacking reflection at 27° 2θ in Figure 1b, suggesting the increased distortion of the stacking arrangement of the carbon nitride layers and the decrease of the crystallite size in the resulting products upon increase of the amount of AgTCM.

To further reveal the nature of the induced chemical changes in the C_3N_4 network, we conducted X-ray photoelectron spectroscopy (XPS) investigations. In Figure 2, the C 1s and N 1s spectra of 2 and 5 wt % AgTCM-mpg-CN are compared to the corresponding spectra of the reference mpg-CN. In general, the C 1s signals of all products (Figure 2a) consist of four contributions, with binding energies of 288.4, 286.5, 284.8, and 282.5 eV. The first one is assigned to CN_3 bonds in the tri-*s*-triazine ring, and the second one to hydroxylated surface carbon atoms (C−OH); the third one is due to adventitious carbon contamination as well as electron-rich sp^2-hybridized carbons (C−C) in the case of AgTCM-modified products,

DOI: 10.1021/acsnano.5b04210
ACS Nano 2016, 10, 3166−3175

while the last contribution suggests the presence of carbide-like carbon (highly negative carbons) in the samples. N 1s signals (Figure 2b) can be deconvolved into four peaks at 400.8 eV (NH_x groups), 399.6 eV (tertiary nitrogens, NC_3, corresponding to the N atoms in the center of the tri-*s*-triazine ring and in tertiary amide group bridging three tri-*s*-triazine units), 398.4 eV (C−N=C, ring nitrogen), and 396.6 eV (negatively charged nitrogen atoms, $C-N^{\ominus}-C$). The negative charge at nitrogen and carbon atoms at the surface of mpg-CN is more pronounced when adding the AgTCM: the weight of the N 1s contribution at 396.6 eV relative to the weight of the main contribution at 398.4 eV is 0.18 for mpg-CN, while in 2- and 5%-doped products, it is 0.62 and 0.89, respectively. On the other hand, in 5 wt % AgTCM-mpg-CN, the weight of the $C^{\ominus}$ contribution at 282.5 eV relative to the weight of the main peak at 288.4 eV is 0.30, while it is only 0.20 in the reference mpg-CN.

We take the increased number of negatively charged carbon and nitrogen atoms in AgTCM-doped CN polymers as an indication for the successful incorporation of tricyanomethanide fragments into a joint electronic network. The fact that more negative charge is localized at nitrogen compared to carbon can be simply explained by its higher electronegativity, which influences the structure of the frontier orbitals.[31] Interestingly, the amounts of the generated formal $N^{\ominus}$ and $C^{\ominus}$ centers greatly exceed those expected according to the quantities of the dopant used in the synthesis. Taking into account that some negatively charged species are characteristic also for the pristine mpg-CN, we suggest that the addition of the tricyanomethanide anion during the synthesis further enhances the tendency of the formation of negatively charged CN polymer structures, where the charges, of course, are delocalized and shared in the joint electron pool by a number of atoms. It will be shown that these negatively charged centers discussed above facilitate the subsequent deposition of metal nanoparticles at the surface of the solids and enhance their catalytic performance.

XPS investigations further confirmed the successful introduction of silver in the products. As shown in Figure S1a, the Ag 3d signal consists of two contributions, a minor one of Ag^+ at 365.8 eV (for $3d_{5/2}$ orbitals) and the major one of Ag^0 at 367.9 eV, which is due to the ammonia-assisted thermal reduction of Ag^+, but potentially also due to electron back-donation from the very electron rich semiconductor framework which can be understood as a macro-version of a ligand. The relative content of pro-forma Ag^0 and Ag^+ estimated according to the areas of the corresponding contributions is 0.61 and 0.39 in 2 wt % AgTCM-mpg-CN and 0.68 and 0.32 in 5 wt % doped product, while absolute weight content of Ag in the surface layer of the samples was calculated as 1.32 and 3.48%, respectively. In order to access the bulk distribution of Ag, a surface layer of the 2 wt % AgTCM-mpg-CN sample was removed by Ar^+ sputtering. It turned out that the Ag content in the bulk of the material is higher than that at the surface, and that Ag^+ ions prevail over Ag^0 (Figure S1a). The enrichment of Ag in the bulk of the products explains the apparent differences in the values of Ag content determined by energy-dispersive X-ray spectroscopy (EDS) and XPS measurements (Table S1). Besides, all the products contain some oxygen, presumably originating mainly from the aqueous workup (Table S1). The O 1s signal consists of the three contributions at 529.4, 531.0, and 532.5 eV due to deprotonated oxygen atoms, surface hydroxyl groups, and surface-adsorbed water, respectively (Figure S1b). The contribution of $O^{\ominus}$ ions increases upon an increase of the AgTCM doping level in the materials; however, taking into account that the total oxygen content in the products is much lower than the sum of nitrogen and carbon content, we expect that the impact of $O^{\ominus}$ groups has minor relevance compared to those of $N^{\ominus}$ and $C^{\ominus}$.

High-angle annular dark-field scanning transmission electron microscopy (HAADF-STEM) investigations performed on an aberration-corrected microscope showed the presence of silver in an atomically dispersed form throughout the samples, clearly seen due to the atomic number (Z) contrast (Figure 3a; see also Figure S2). The absence of diffraction rings corresponding to crystalline Ag (inset Figure 3a) gives further verification that Ag atoms are ubiquitously dispersed and not in the form of nanoparticles. This is additionally supported by the HAADF-STEM image obtained on a standard microscope along with EDS mapping of C, N, and Ag, which shows the homogeneous distribution of these elements (Figure 3b−e). The energy-dispersive X-ray spectrum retrieved from the collected data of these maps (Figure 3f) confirms the presence of all relevant elements in this area. No regions of pronounced local intensity are seen in the Ag map (Figure 3e), verifying the absence of

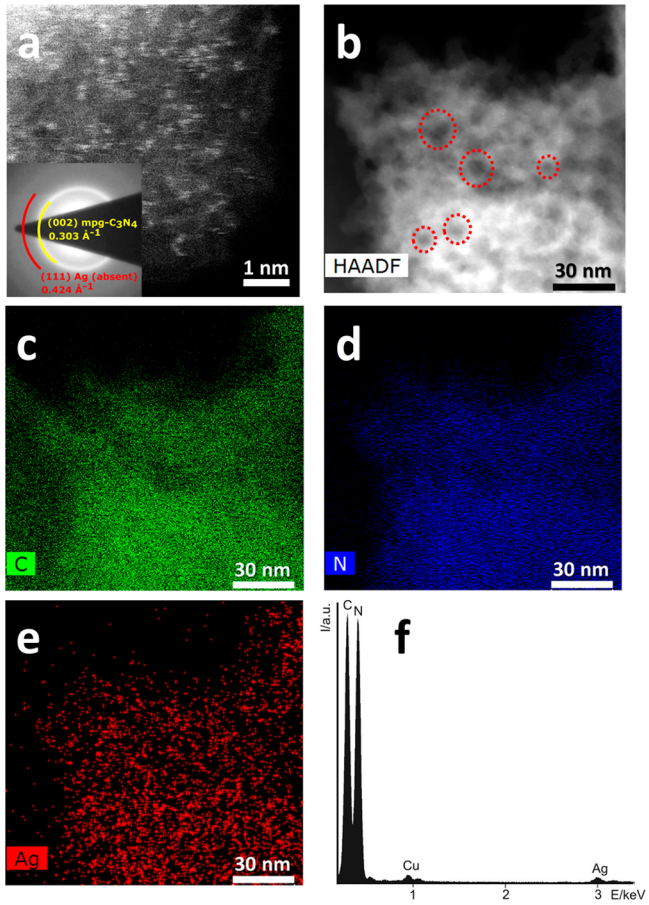

Figure 3. (a) Aberration-corrected HAADF-STEM image of the 1 wt % AgTCM-mpg-CN, showing isolated single Ag atoms distributed across the mpg-CN support. Inset: Diffraction pattern from this sample. (b) Low-magnification HAADF-STEM image (a few selected mesopores are indicated by dashed circles) along with C (c), N (d), and Ag (e) EDS mapping of 2 wt % AgTCM-mpg-CN. EDS spectrum extracted from the map data. The Cu peak is due to the material of the TEM grid (f).

DOI: 10.1021/acsnano.5b04210
ACS Nano 2016, 10, 3166−3175

nanoparticles. Instead, Ag is detected to be nearly uniformly distributed across the mpg-CN support. It is remarkable that, upon increase of silver content in the products, no major Ag NPs are detected, as shown by the analysis of 10 wt % AgTCM-mpg-CN (see Figure S3). Additionally, the HAADF-STEM micrographs enable visualization of the characteristic mesopores of 5−25 nm of the solids, in line with the results of N_2 physisorption studies (see below).

ζ-Potential measurements also reflect the influence of the introduced negatively charged centers on the surface properties of the prepared solids. The isoelectric point (IEP) of reference mpg-CN is found to be 2.56, which is usually attributed to the presence of the surface hydroxyl groups (C−OH) that are highly acidic and dissociate in water to give surface $O^{\ominus}$ ions.[32,33] Upon increasing the AgTCM content, the isoelectric point of the corresponding products, however, shifts to even lower values, and the IEP can be as low as 1.83 for 10 wt % AgTCM-mpg-CN (Figure S4). We attribute that to the strongly stabilized negative charge on the structure which cannot be easily neutralized by protons, which can also be described as an increased, presumably nonlocalized, basicity of the surface.

One nearby advantage of the described TCM doping method over the already reported approaches is that the AgTCM-doped products possess up to 1.5 times higher surface areas compared to the reference mpg-CN, as delineated in Table 1 and Figure 4a. The increase of the surface areas is accompanied by the increase of the pore volumes, resulting from the increased size of the generated pores as suggested by the slight shift of the hysteresis onset in the corresponding nitrogen sorption isotherms to higher p/p_0 as well as by the results of pore size analysis (Figure 4a,b). AgTCM-doped products are characterized by more homogeneous pore size distribution than the reference mpg-CN that follows from almost vertical inclination of the sorption curves at p/p_0 = 0.65−0.95 and points out the beneficial effect of silver doping. There is a minor development of microporosity when silver is introduced in the materials. Tentatively, this could be related to the disturbance of the local carbon nitride network structure by the Ag species or to the stabilization of micropores by Ag species, but understanding of the phenomenon is beyond the scope of the present contribution.

Table 1. Physical and Textural Properties of the Reference mpg-CN and AgTCM-Doped Products as Well as Measured Hydrogen Evolution Rates of These Materials

product	S_{BET}[a] (m^2/g)	V_{pore}[b] (cm^3/g)	V_{micro}[c] (cm^3/g)	BG[d] (eV)	HER[e] (μmol/h)
ref mpg-CN	119	0.223	0.007	2.78	9.8
1% AgTCM-mpg-CN	193	0.354	0.009	2.79	35.5
2% AgTCM-mpg-CN	157	0.510	0.009	2.78	39.5
3.5% AgTCM-mpg-CN	206	0.759	0.010	2.75	36.9
5% AgTCM-mpg-CN	190	0.690	0.010	2.73	29.2
10% AgTCM-mpg-CN	188	0.676	0.009	2.67	21.2

[a]Total surface area. [b]Pore volume at p/p_0 = 0.95. [c]The *t*-plot method. [d]Optical band gap. [e]Measured hydrogen evolution rate.

The influence of the negatively charged species on the electronic properties of the C_3N_4 structure introduced by TCM doping was examined by optical spectroscopy, electrochemical impedance spectroscopy, and Mott−Schottky analysis. First, the controlled insertion of carbon−carbon bonds (Scheme 1) enables the tuning of the visible light absorption properties of the resulting CN polymers and their optical band gap values, as shown in Figure 5a: with increasing AgTCM concentration, the visible light absorption threshold shifts slightly to longer wavelengths. Furthermore, the successful introduction of silver species and partial negative charges into the carbon nitride network results in an increase of the steady-state photoluminescence (PL) for almost all of the products (Figure 5b). A clear red shift is observed in the emission spectra, and it gets more pronounced with increasing dopant quantity. At the same time, PL lifetime is almost unaltered, as shown in Figure S5, for the comparison of the 3.5 wt % AgTCM-doped product and the reference mpg-CN. Such a combination illustrates a change of the semiconductor behavior which is rather untypical for the conventional CN polymers, where the reported structural defects are mainly deep-level traps at which nonradiative recombination occurs, and the decrease of PL lifetime is accompanied by a decrease of the steady-state PL.[34] One might speculate that the red-shifted states introduced by doping promote recombination of electrons and holes by their colocalization at the silver centers due to tighter binding. The significant decrease of PL upon increasing AgTCM concentration to 10 wt % is caused by introduction of lattice defects, as corroborated by PXRD investigations.

Despite the induced chemical modifications, Mott−Schottky analysis indicated that the absolute values of flat-band potentials

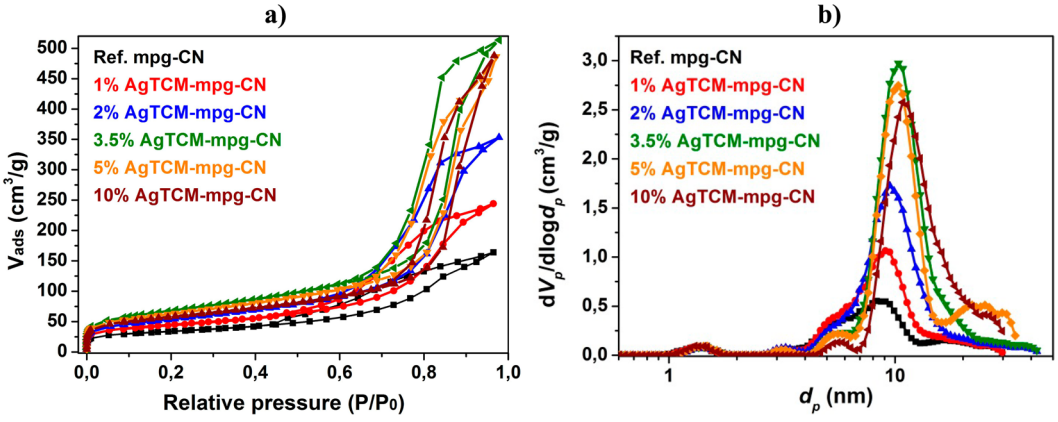

Figure 4. Nitrogen sorption isotherms at 77 K (a) and corresponding pore size distribution calculated by a nonlocal density functional theory model assuming slit-shaped pores (b) of the reference mpg-CN and Ag-containing materials.

DOI: 10.1021/acsnano.5b04210
ACS Nano 2016, 10, 3166−3175

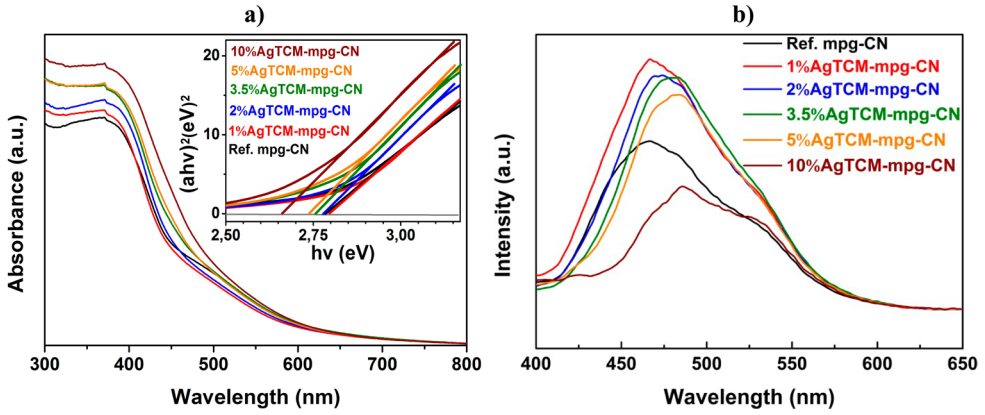

Figure 5. UV−vis absorption spectra of AgTCM-doped products illustrating improvement of visible light absorption upon increasing amount of the dopant (a); emission spectra of the reference mpg-CN and AgTCM-doped products excited at 350 nm (b).

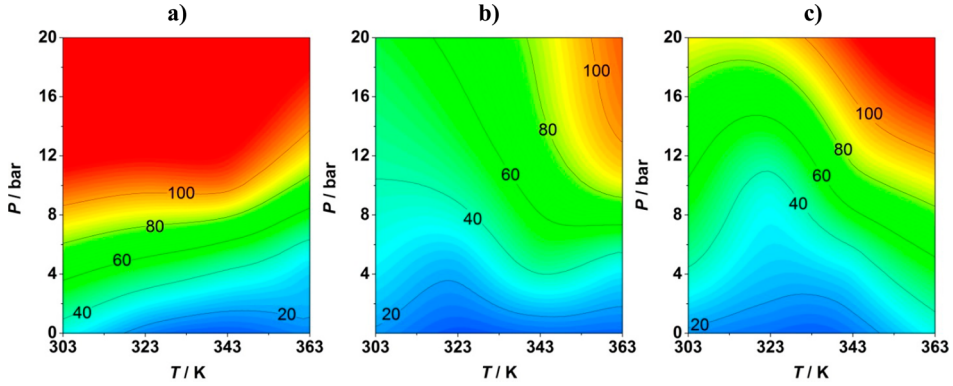

Figure 6. Rate of 1-hexyne hydrogenation (in mol_{alkyne} h^{-1} mol_{Ag}^{-1}) at different temperatures and pressures over AgTCM-mpg-CN (a), Ag-mpg-CN-SD (b), and Ag-mpg-CN-IR (c). Reaction conditions: W_{cat} = 200 mg, F(1-hexyne + toluene) = 1 cm^3 min^{-1}, $F(H_2)$ = 36 cm^3 min^{-1}. The selectivity to 1-hexene was 100% in all three cases.

of AgTCM-doped products are very close to that of the reference mpg-CN (which is about −0.83 eV on the RHE scale). This might be due to the compensation of the effects of Ag^+ introduced mainly to the bulk of products (as supported by ^{13}C NMR and Ag 3d XPS spectra after bombardment) by negatively charged nitrogen and carbons located preferentially in the surface layer (as seen from ζ-potential values and C 1s and N 1s XPS spectra). All samples showed a positive slope in the linear Mott−Schottky plots (Figure S6a), which is characteristic for n-type semiconductors and goes well with the excess negative charges on the semiconductor framework. This suggests that the found values of flat-band potentials approximately correspond to the conduction band positions of the materials. The positions of the valence bands were estimated by subtraction of the optical band gap values from the flat-band potentials; the obtained results are indicated in Figure S6b.

As a result of superposition of favorable material properties provided by TCM doping, namely, increased surface areas, created negatively charged surface sites for charge exchange, and despite lower X-ray structural order, AgTCM-mpg-CN products show an activity in the Pt-assisted photocatalytic water reduction up to 4 times higher than that of the reference mpg-CN sample (Figure S7a and Table 1). The detailed description of the experimental procedure is given in the Materials and Methods section. In the beginning of the sacrificial water reduction experiments, hexachloroplatinic acid is added and photoreduced, yielding Pt NPs that are *in situ* deposited on the electron exit sites of the surface of the photocatalyst. EDS investigations of the photocatalysts after hydrogen evolution reaction showed that the amount of Pt deposited at the surface of 3.5% AgTCM-mpg-CN is 1.47 wt %, which is 2-fold higher than the Pt amount deposited at mpg-CN (0.71 wt %). The highest activity of 39.5 μmol H_2/h is observed for 2 wt % AgTCM-mpg-CN (the value for the reference mpg-CN is 9.8 μmol H_2/h). Further increase of the dopant concentration obviously leads to more significant distortion of the semiconductor lattice, resulting in the decrease of the photocatalytic reaction rates. Pristine AgTCM-mpg-CN photocatalysts without Pt particles are able to reduce water, as well, though with much lower reaction rates compared to Pt-loaded ones. For example, 3.5 wt % AgTCM-mpg-CN produces 1.25 μmol H_2/h (Figure S7b).

Finally, we assessed the catalytic performance of the AgTCM-doped material (1 wt % Ag) in the continuous-flow three-phase semihydrogenation of 1-hexyne, a model reaction for processes used in the manufacture of fine chemicals and pharmaceutical intermediates.[35] For comparison, 1 wt % Ag-loaded mesoporous carbon nitrides prepared by conventional techniques such as spray deposition (coded Ag-mpg-CN-SD)[28,36] and impregnation−chemical reduction (coded Ag-mpg-CN-IR) were evaluated, as well. Details on the preparation and characterization of the latter solids can be found in the Materials and Methods section and in Table S2 (Supporting Information), respectively. In general, these two materials exhibited truncated octahedral-shaped nanoparticles, exposing

DOI: 10.1021/acsnano.5b04210
ACS Nano 2016, 10, 3166−3175

(111) and (100) faces, with an average diameter of approximately 5 nm.

The contour plots in Figure 6 depict the results of the catalytic tests. The AgTCM-doped material is by far the most active catalyst. For example, at 303 K and 10 bar, the reaction rate exceeds 100 mol_{alkyne} h^{-1} mol_{Ag}^{-1} over the AgTCM-doped sample (Figure 6a), while it is *ca.* 40 and 60 mol_{alkyne} h^{-1} mol_{Ag}^{-1} over the materials prepared by spray deposition and impregnation−reduction, respectively (Figure 6b,c). The activity of AgTCM-mpg-CN exceeds, as well, that of the Ag catalysts reported in the literature (*e.g.*, 1 wt % Ag/TiO_2, average silver particle diameter = 5 nm),[36] which yielded *ca.* 30 mol_{alkyne} h^{-1} mol_{Ag}^{-1} at the same conditions. Accordingly, it can be concluded that the extremely high dispersion of the silver atoms in the single-site AgTCM-mpg-CN catalyst leads to a superior catalyst compared to the materials where silver is stabilized as nanoparticles (the latter exposed less surface to the reaction medium per mole of metal). In addition to its remarkable activity, the doped catalyst exhibits also a selectivity of 100% to the desired olefin at all conditions investigated. This is expected for silver catalysts, due to their ability to prevent overhydrogenation and isomerization pathways.[36] Table 2 compares the performance of AgTCM-mpg-CN with a number of benchmark heterogeneous catalysts for the semihydrogenation of 1-hexyne. The single-atom silver catalyst is superior to supported CeO_2 and Au nanoparticles, and it is even competitive with the archetypical Lindlar catalyst (Pd−Pb/$CaCO_3$). We have also included the recently reported Pd-mpg-CN,[37] which comprises single palladium atoms stabilized on the carbon nitride structure. The latter is *ca.* 6 times more active than the silver analogue, which comes as no surprise following the much easier H_2 splitting on Pd compared to Ag.

Table 2. Comparison of Heterogeneous Catalysts in the Semihydrogenation of 1-Hexyne

catalyst	metal loading (wt %)	rate ($mol_{product}$ h^{-1} mol_{metal}^{-1})	S(1-hexene) (%)
AgTCM-mpg-CN[a]	1	103	100
Ag-mpg-CN-SD[a]	1	39	100
Ag/TiO_2[a,28]	1	32	100
Pd−Pb/$CaCO_3$[b,37]	5	101	98
Pd-mpg-CN[b,37]	0.5	578	100
Au/TiO_2[c,28]	1	41	97
CeO_2/TiO_2[d,38]	16	2	100

[a] W_{cat} = 200 mg, T = 303 K, P = 10 bar, F(1-hexyne + toluene) = 1 cm^3 min^{-1}, $F(H_2)$ = 36 cm^3 min^{-1}. [b] W_{cat} = 100 mg, T = 303 K, P = 1 bar, F(1-hexyne + toluene) = 1 cm^3 min^{-1}, $F(H_2)$ = 24 cm^3 min^{-1}. [c] W_{cat} = 100 mg, T = 373 K, P = 10 bar, F(1-hexyne + toluene) = 1 cm^3 min^{-1}, $F(H_2)$ = 36 cm^3 min^{-1}. [d] W_{cat} = 850 mg, T = 363 K, P = 40 bar, F(1-hexyne + toluene) = 0.3 cm^3 min^{-1}, $F(H_2)$ = 36 cm^3 min^{-1}.

At this point, we should note that, compared to the reported preparation of carbon nitride supported single-atom-dispersed Pd by an impregnation−chemical reduction procedure,[37] the metal tricyanomethanide copolymerization approach offers the following advantages: first, the introduction of negatively charged C and N atoms in the C_3N_4 network (Scheme 1) enables better dispersion of metal species (as metal atoms, ions, or clusters) in the products. Even at 10 wt % dopant concentration, no agglomeration of Ag to Ag NPs was detected in the products. The introduction of similar metal amounts by the impregnation−chemical reduction procedure leads to the formation of metal NPs due to insufficient stabilization of single metal atoms/ions by the support.[23] Furthermore, the TCM−copolymerization approach enables one to obtain materials having a joint electronic system and thus featuring very unusual hybrid material properties (*e.g.*, increased PL). The use of the reactive precursor and the fact that AgTCM is soluble in molten cyanamide ensures homogeneity of metal distribution within the products. Finally, in contrast to the impregnation−chemical reduction procedure, the suggested method of metal introduction leads to products with a 50% increase of BET surface areas compared to that of the reference (nondoped) mpg-CN.

Table 2 clearly demonstrates that single-atom catalysts show enhanced reactivity compared to nanoparticle-based catalysts as a consequence of their dispersion of the active phase, leading to a very high metal utilization in the catalytic process. A single-site silver catalyst competes with a conventional nanoparticulate palladium catalyst in terms of reactivity and selectivity (see Table 2 to compare the performance of AgTCM-mpg-CN with that of Pd−Pb). For a silver catalyst comprising silver nanoparticles, such competitive performance is not observed (see Table 2 to compare the performance of Ag-mpg-CN-SD with that of Pd−Pb). Thus, by creating single-atom catalytic centers, an intrinsically unreactive metal such as silver can approach the activity of the most active hydrogenation catalyst (*i.e.*, Pd-based). It should be also taken into account that Ag is much cheaper than Pd.

The role of the negatively charged carbon nitride support in the catalytic cycle (*e.g.*, partaking in H_2 splitting and/or alkyne adsorption) can also contribute to this improved performance. However, blank experiments over the silver-free carbon nitride revealed its complete inactivity under the studied experimental conditions, emphasizing the primary role of the silver atoms in the observed catalytic behavior. Future studies should carefully address the nature of the active silver species in the reaction. XPS analyses have demonstrated two different states of silver (metallic and charged atoms). Ag^0 is often regarded as the active hydrogenation phase.[28,36] However, our recent communication dealing with atomic Pd stabilized on mesoporous carbon nitride hinted a possible beneficial contribution of charged atoms in alkyne hydrogenation.[37] Discriminating between the relative importance of the metallic/ionic state of silver (or a different atom) in the hydrogenation process is beyond the scope of this paper and would require dedicated operando spectroscopic investigations. Detailed density functional theory analyses of the reaction mechanism over these cationic−anionic polarized surface patterns of the carbon nitride support will also contribute to further understand these intriguing materials.

CONCLUSION

The modification of a carbon nitride structure by doping with silver tricyanomethanide leads to the creation of extra negatively charged/polarized carbon and nitrogen centers, neutralized by silver ions, which are atomically dispersed within the structure. All applied techniques indicate that silver plays the role of a highly efficient dopant for carbon nitride and gets hybridized into the resulting electronic network with a shared electron orbital structure. The obtained solids possess comparably high surface areas and are characterized by homogeneous distribution of silver present as atomic dispersion in the final products. The usefulness of this material was illustrated in two applications: the photoassisted water

DOI: 10.1021/acsnano.5b04210
ACS Nano 2016, 10, 3166−3175

reduction (after further Pt NP deposition) and the selective hydrogenation of 1-hexyne. The simultaneous insertion of a metal species from a TCM precursor, if combined with a proper selection of the reaction atmosphere (inert, oxidative, or reductive), is expected to be a general way to prepare various single-site metal-supported organocatalysts for diverse applications.

MATERIALS AND METHODS

Materials. Cyanamide (99%), silver nitrate ($AgNO_3$, 99%), LUDOX HS-40 colloidal silica, ammonium hydrogen difluoride (NH_4HF_2, 99%), and hexachloroplatinic acid (H_2PtCl_6) solution (8 wt % aqueous solution) were purchased from Sigma-Aldrich, and triethanolamine (98%) was purchased from Alfa Aesar. Sodium tricyanomethanide (NaTCM) was received as a gift from Lonza AG. All chemicals were of analytical grade and used without further purification.

Synthesis of Silver Tricyanomethanide. NaTCM (6.005 g, 53.1 mmol) was dissolved in 12 mL of water (solution 1), and 9.106 g of $AgNO_3$ (53.1 mmol) was dissolved in 18 mL of water (solution 2); solutions were heated to 80 °C in a preheated oven. Afterward, hot solution 2 was added to hot solution 1 dropwise under vigorous stirring, and then the reaction flask was wrapped with Al foil and left upon agitation overnight at room temperature. The obtained white precipitate was filtered off, rinsed with deionized water, and then dried at 60° under vacuum (0.5 mbar).

Synthesis of AgTCM-mpg-CN. The AgTCM-doped mpg-CN samples were prepared by dispersing 1250 mg (29.4 mmol) of cyanamide and different amounts of AgTCM (12.5, 25, 43.8, 62.5, and 125 mg for 1, 2, 3.5, 5, and 10 wt % AgTCM-mpg-CN samples) in 2−3 mL of water. Then, appropriate amounts of a 40% dispersion of 12 nm colloidal silica (LUDOX HS-40) were added, and reagent mixtures were stirred at 100 °C for several hours to evaporate water. The weight ratio between precursors and silica was always fixed to 1:1. The resultant white powder was ground thoroughly and then heated to 550 °C at a heating rate of 2.3 °C/min and maintained for 4 h at 550 °C under a flow of nitrogen (15 L/min). The obtained brown-yellow powders were washed with 4 M NH_4HF_2 solution for 48 h to remove the silica template. Afterward, the powders were filtered, washed with water and ethanol several times until neutral pH, and finally dried under vacuum (10 mbar) at 50 °C overnight. The reference mpg-CN was prepared by the same procedure but without using AgTCM.

The reference mesoporous graphitic carbon nitride (mpg-CN) was prepared in exactly the same way and under the same conditions but without using AgTCM. The preparation procedure is described elsewhere.[29]

Synthesis of 1 wt % Ag-mpg-CN by an Impregnation−Reduction Method (Ag-mpg-CN-IR). Typically, 2 g of mpg-CN was dispersed in 200 mL of deionized (DI) water under sonication for 30 min. Then 31.5 mg of $AgNO_3$ was added into the suspension for impregnation, followed by another 30 min sonication. Afterward, 5.6 mL of freshly prepared 0.5 M $NaBH_4$ solution in DI water was added into the suspension under vigorous stirring. The reaction mixture was agitated overnight. The final 1% Ag-mpg-CN-IR was separated by filtration, washed with DI water and ethanol thoroughly, and dried under vacuum (10 mbar) at 50 °C.

Synthesis of 1 wt % Ag-mpg-CN by Spray Deposition (Ag-mpg-CN-SD).[39] The preparation was carried out in a Büchi mini spray dryer B-290 equipped with a two-fluid nozzle with a 1.4 mm diameter. This technique allows the deposition of metal (oxide) particles with a high degree of dispersion. Silver nitrate (0.01 g) was dissolved in 20 cm^3 of DI water under magnetic stirring at room temperature, followed by addition of the support (mpg-CN, 1 g). The resulting suspension was pumped at 3 $cm^3\ min^{-1}$ into the two-fluid nozzle, together with a spray air flow of 0.5 $m^3\ h^{-1}$, creating droplets of 20−30 μm. The inlet temperature was set at 493 K, the aspiration rate at 35 $m^3\ h^{-1}$, and the outlet temperature at 383 K. The dried particles were separated using a cyclone and activated in 5 vol % H_2/N_2 (20 $cm^3\ min^{-1}$) at 473 K for 30 min.

Photocatalytic Hydrogen Evolution Tests. Reactions were performed using a side-irradiated closed steel reactor equipped with a Teflon inlet, thermocouple, pressure sensor, magnetic stirring, and thermostat and connected to a Schlenk line. H_2 production was carried out using 50 mg of catalyst dispersed in 38 mL of solvent mixture composed of triethanolamine and water in the ratio of 1/9 (v/v). Pt nanoparticles (3 wt %) were deposited on carbon nitrides by an *in situ* photodeposition procedure using hexachloroplatinic acid (H_2PtCl_6) solution as a precursor. The buildup of H_2 pressure was monitored as a function of the irradiation time. The irradiation source was a 50 W white LED array (Bridgelux BXRA-50C5300, λ > 410 nm). The detailed description of the setup and the test procedure can be found in the literature.[40]

Characterization. Powder X-ray diffraction patterns were measured on a Bruker D8 Advance diffractometer equipped with a scintillation counter detector with Cu Kα radiation (λ = 0.15418 nm) applying a 2θ step size of 0.05° and counting time of 4 s per step. The solid-state NMR $^{13}C\{^1H\}$ CP/MAS (cross-polarization magic angle spinning) measurements were carried out using a Bruker Avance 400 spectrometer operating at 100.6 MHz using a Bruker 4 mm double-resonance probe head operating at a spinning rate of 10 kHz. ^1H composite pulse decoupling was applied during the acquisition. ^{13}C chemical shifts were referenced externally to tetramethylsilane using adamantane as a secondary reference. Nitrogen sorption at 77 K was measured in a Micromeritics 3Flex instrument. Prior to the measurement, the samples were evacuated at 423 K for 6−7 h until a residual pressure of 10^{-8} bar was reached. The surface area was determined *via* the BET method, and the *t*-plot method was used to discriminate between the micro- and mesopores. The nonlocal density functional theory model was used to calculate the pore size distributions, assuming slit-shaped pores.[41,42] Elemental analysis was accomplished as combustion analysis using a Vario microdevice. Optical absorbance spectra of powders were measured on a Shimadzu UV 2600 equipped with an integrating sphere. The emission spectra were recorded on LS-50B PerkinElmer instrument. The excitation wavelength was 350 nm. Time-resolved photoluminescence measurements were carried out at room temperature using the Edinburgh Instruments (FLSP 920) system, equipped with a 450 W xenon lamp as the excitation source. Scanning electron microscopy images were obtained on a LEO 1550-Gemini microscope. The scanning transmission electron microscopy investigations were performed on an aberration-corrected HD-2700CS (Hitachi; cold-field emitter) operated at an acceleration potential of 200 kV,[43] as well as an aberration-corrected Titan cubed microscope operated at 300 kV (FEI; ultrahigh brightness X-FEG electron source) with an illumination angle of 20.6 mrad and probe current of *ca.* 60 pA. The probe correctors (CEOS) incorporated in these microscope columns provide atomic-resolution capability (beam diameter *ca.* 0.1 nm). Images (1024 × 1024 pixels) were recorded with a HAADF detector with frame times of *ca.* 15 s. These imaging conditions give rise to atomic number (*Z*) contrast, a highly sensitive method to detect atoms of strongly scattering elements (high *Z*) on light supports. STEM combined with EDS was performed on a Talos microscope (FEI; high brightness field emission gun), operated at an acceleration potential of 200 kV. Four EDS detectors were attached to this microscope, allowing one to record EDS maps with good signal-to-noise ratio in relatively short time (here 10−20 min). XPS was performed on a Multilab 2000 (Thermo) spectrometer equipped with Al Kα anode ($h\nu$ = 1486.6 eV). All spectra were referenced to the C 1s peak of adventitious carbon at 284.8 eV. For quantification purposes, survey spectra at a pass energy of 50 eV and high-resolution spectra at a pass energy of 20 eV were recorded and analyzed by XPS Peak 4.1 software (written by Raymund Kwok). The spectra were decomposed assuming line shapes as sum functions of Gaussian (80%) and Lorentzian (20%) functions. Raw areas determined after subtraction of a Shirley background[44] were corrected according to following sensitivity factors[45] (C 1s, 0.25; N 1s, 0.42; O 1s, 0.66; Ag 3d, 5.2). Etching Ar^+ bombardment was performed at 2 kV and 18 mA of ionic current. ζ-Potential measurements were performed using Zetasizer nano ZS, and the data analysis was conducted by using "Zetasizer" software.

DOI: 10.1021/acsnano.5b04210
ACS Nano 2016, 10, 3166−3175

Mott–Schottky analysis was performed by measuring impedance spectra of the samples in a potential range from 0.30 to −0.60 V RHE, −0.02 V potential step, and frequencies from 10 kHz to 0.1 Hz, 7 mV potential amplitude. The measurements were performed in a standard three-compartment electrochemical cell. Pt coil and mercury sulfate electrodes were utilized as counter and reference electrodes correspondingly. The curves are presented in reversible hydrogen electrode scale RHE (0.000 V RHE = −0.635 V Ag/AgCl for pH 7.0). The measurements were performed in 0.1 M phosphate buffer solution with pH 7.0. The solution was purged by N_2 before the measurements to remove oxygen; a constant flow of N_2 was kept during the measurements in order to avoid oxygen leaking into the cell. The electrodes were prepared by deposition of a known amount of the powder on a Au substrate. Au was chosen as a substrate electrode due to its (1) low interfacial capacity comparing to other typical substrates, such as carbon or metal oxides (ITO, FTO), (2) high surface roughness, and (3) positive surface charge helping to improve the adhesion of powder samples, whose surface is negatively charged. In order to prepare the electrode, the known amount of powder was ultrasonically dispersed in ethanol in order to make 100 mg/mL ink. Then 100 μL of ink was deposited on the Au substrate in five steps with drying in air between the steps. Finally, 40 μL of 5% solution of Nafion in ethanol was pipetted on the deposit to avoid its detachment. Preliminary experiments with pure Au substrate and Au + Nafion electrode were performed to demonstrate their negligible contribution into the measured capacity of electrodes with deposited sample powder.

Measured impedance spectra were fitted with the simplest equivalent circuit capable of fitting experimental data: $R_1(CR_2)$. Here R_1 is related to the resistance of the electrolyte, R_2 is charge transfer resistance due to reduction of residual oxygen and/or evolution of hydrogen (close and below 0,00 V RHE), C is an interfacial capacity predominantly determined by space charge layer in the semiconducting electrode.[46] In order to take into account frequency dispersion of C due to surface inhomogeneity, the capacity was modeled as constant phase element Q ($-Z'' = 1/C(j\omega)^{\alpha}$) with fixed phase shift constant $\alpha = 0.90$.

Hydrogenation of 1-Hexyne. The hydrogenation of 1-hexyne (Acros Organics, 98%) was carried out in a continuous-flow flooded-bed microreactor (ThalesNano H-Cube Pro), in which the liquid alkyne and the gaseous hydrogen (produced *in situ* by Millipore water electrolysis) flow concurrently upward through a fixed catalytic bed, contained in a cartridge of approximately 3.5 mm in diameter, and composed of 0.2 g of catalyst. The liquid feed contained 5 vol % of substrate and toluene (Fischer Chemicals, 99.95%) as solvent. The reactions were conducted at various conditions of temperature (303–363 K) and total pressure (1–20 bar) and at constant liquid (1 cm^3min^{-1}) and H_2 (36 cm^3min^{-1}) flow rates. The reaction products were collected by employing an autosampler, after reaching in 15 min steady-state operation, and analyzed offline using a gas chromatograph (HP-6890) equipped with a HP-5 capillary column and a flame ionization detector. The reaction rate was expressed as the number of moles of product per mole of metal and unit time. The selectivity to 1-hexene, S(1-hexene), was quantified as the amount of the 1-hexene produced divided by the amount of reacted alkyne.

ASSOCIATED CONTENT

Supporting Information

The Supporting Information is available free of charge on the ACS Publications website at DOI: 10.1021/acsnano.5b04210.

Elemental composition of the reference mesoporous graphitic carbon nitride (ref mpg-CN) and AgTCM-doped mpg-CN products; Ag 3d and O 1s XPS spectra as well as the relative content of different C, N, and O contributions in the selected samples; ζ-potentials at different pH values and estimated values of isoelectric points of the reference mpg-CN and AgTCM-doped products; time-resolved photoluminescence spectra of the ref mpg-CN and 3.5% AgTCM-mpg-CN; Mott–Schottky plots and band positions of the ref mpg-CN and the selected AgTCM-doped products; time course of H_2 evolution reactions using ref mpg-CN and AgTCM-doped solids with and without Pt assistance; composition and textural properties of catalysts used for hydrogenation studies (PDF)

AUTHOR INFORMATION

Corresponding Author

*E-mail: dariya.dontsova@mpikg.mpg.de.

Present Address

¶Institute of Nano Science and Technology (INST), Habitat Centre, Phase-10, Sector-64, Mohali, 160062 Punjab, India.

Notes

The authors declare no competing financial interest.

ACKNOWLEDGMENTS

Prof. Hua Gui Yang is acknowledged for PL lifetime measurements. The Scientific Center for Optical and Electron Microscopy (ScopeM) at ETH Zurich is acknowledged for providing access to the facilities.

REFERENCES

(1) Martin, D. J.; Reardon, P. J. T.; Moniz, S. J. A.; Tang, J. Visible Light-Driven Pure Water Splitting by a Nature-Inspired Organic Semiconductor-Based System. *J. Am. Chem. Soc.* **2014**, *136*, 12568–12571.

(2) Maeda, K.; Wang, X.; Nishihara, Y.; Lu, D.; Antonietti, M.; Domen, K. Photocatalytic Activities of Graphitic Carbon Nitride Powder for Water Reduction and Oxidation under Visible Light. *J. Phys. Chem. C* **2009**, *113*, 4940–4947.

(3) Wang, X.; Maeda, K.; Thomas, A.; Takanabe, K.; Xin, G.; Carlsson, J. M.; Domen, K.; Antonietti, M. A Metal-Free Polymeric Photocatalyst for Hydrogen Production from Water under Visible Light. *Nat. Mater.* **2009**, *8*, 76–80.

(4) Thomas, A.; Fischer, A.; Goettmann, F.; Antonietti, M.; Muller, J.-O.; Schlogl, R.; Carlsson, J. M. Graphitic Carbon Nitride Materials: Variation of Structure and Morphology and Their Use as Metal-Free Catalysts. *J. Mater. Chem.* **2008**, *18*, 4893–4908.

(5) Wang, X.; Chen, X.; Thomas, A.; Fu, X.; Antonietti, M. Metal-Containing Carbon Nitride Compounds: A New Functional Organic–Metal Hybrid Material. *Adv. Mater.* **2009**, *21*, 1609–1612.

(6) Li, X.; Guo, Z.; Li, J.; Zhang, Y.; Ma, H.; Pang, X.; Du, B.; Wei, Q. Quenched Electrochemiluminescence of Ag Nanoparticles Functionalized g-C_3N_4 by Ferrocene for Highly Sensitive Immunosensing. *Anal. Chim. Acta* **2015**, *854*, 40–46.

(7) Xu, L.; Li, H.; Xia, J.; Wang, L.; Xu, H.; Ji, H.; Li, H.; Sun, K. Graphitic Carbon Nitride Nanosheet Supported High Loading Silver Nanoparticle Catalysts for the Oxygen Reduction Reaction. *Mater. Lett.* **2014**, *128*, 349–353.

(8) Bai, X.; Zong, R.; Li, C.; Liu, D.; Liu, Y.; Zhu, Y. Enhancement of Visible Photocatalytic Activity *via* Ag@C_3N_4 Core–Shell Plasmonic Composite. *Appl. Catal., B* **2014**, *147*, 82–91.

(9) Jiang, D.; Zhang, Y.; Chu, H.; Liu, J.; Wan, J.; Chen, M. N-doped Graphene Quantum Dots as an Effective Photocatalyst for the Photochemical Synthesis of Silver Deposited Porous Graphitic C_3N_4 Nanocomposites for Nonenzymatic Electrochemical H_2O_2 Sensing. *RSC Adv.* **2014**, *4*, 16163–16171.

(10) Bu, Y.; Chen, Z.; Li, W. Using Electrochemical Methods to Study the Promotion Mechanism of the Photoelectric Conversion Performance of Ag-Modified Mesoporous g-C_3N_4 Heterojunction Material. *Appl. Catal., B* **2014**, *144*, 622–630.

(11) Peng, H.; Mo, Z.; Liao, S.; Liang, H.; Yang, L.; Luo, F.; Song, H.; Zhong, Y.; Zhang, B. High Performance Fe- and N- Doped Carbon

DOI: 10.1021/acsnano.5b04210
ACS Nano 2016, 10, 3166–3175

Catalyst with Graphene Structure for Oxygen Reduction. *Sci. Rep.* **2013**, *3*, 1765.
(12) Ge, L.; Han, C.; Liu, J.; Li, Y. Enhanced Visible Light Photocatalytic Activity of Novel Polymeric g-C_3N_4 Loaded with Ag Nanoparticles. *Appl. Catal., A* **2011**, *409*−*410*, 215−222.
(13) Katsumata, H.; Sakai, T.; Suzuki, T.; Kaneco, S. Highly Efficient Photocatalytic Activity of g-C_3N_4/Ag_3PO_4 Hybrid Photocatalysts through Z-Scheme Photocatalytic Mechanism under Visible Light. *Ind. Eng. Chem. Res.* **2014**, *53*, 8018−8025.
(14) Jiang, D.; Zhu, J.; Chen, M.; Xie, J. Highly Efficient Heterojunction Photocatalyst Based on Nanoporous g-C_3N_4 Sheets Modified by Ag_3PO_4 Nanoparticles: Synthesis and Enhanced Photocatalytic Activity. *J. Colloid Interface Sci.* **2014**, *417*, 115−120.
(15) Kumar, S.; Surendar, T.; Baruah, A.; Shanker, V. Synthesis of a Novel and Stable g-C_3N_4-Ag_3PO_4 Hybrid Nanocomposite Photocatalyst and Study of the Photocatalytic Activity under Visible Light Irradiation. *J. Mater. Chem. A* **2013**, *1*, 5333−5340.
(16) Yang, X.; Tang, H.; Xu, J.; Antonietti, M.; Shalom, M. Silver Phosphate/Graphitic Carbon Nitride as an Efficient Photocatalytic Tandem System for Oxygen Evolution. *ChemSusChem* **2015**, *8*, 1350−1358.
(17) Ren, H.-T.; Jia, S.-Y.; Wu, Y.; Wu, S.-H.; Zhang, T.-H.; Han, X. Improved Photochemical Reactivities of Ag_2O/g-C_3N_4 in Phenol Degradation under UV and Visible Light. *Ind. Eng. Chem. Res.* **2014**, *53*, 17645−17653.
(18) Jiang, D.; Chen, L.; Xie, J.; Chen, M. Ag_2S/g-C_3N_4 Composite Photocatalysts for Efficient Pt-free Hydrogen Production. The co-catalyst Function of Ag/Ag_2S Formed by Simultaneous Photodeposition. *Dalton Trans.* **2014**, *43*, 4878−4885.
(19) Bu, Y.; Chen, Z.; Feng, C.; Li, W. Study of the Promotion Mechanism of the Photocatalytic Performance and Stability of the Ag@AgCl/g-C_3N_4 Composite under Visible Light. *RSC Adv.* **2014**, *4*, 38124−38132.
(20) Cao, J.; Zhao, Y.; Lin, H.; Xu, B.; Chen, S. Ag/AgBr/g-C_3N_4: A Highly Efficient and Stable Composite Photocatalyst for Degradation of Organic Contaminants under Visible Light. *Mater. Res. Bull.* **2013**, *48*, 3873−3880.
(21) Xu, Y.-S.; Zhang, W.-D. Ag/AgBr-Grafted Graphite-like Carbon Nitride with Enhanced Plasmonic Photocatalytic Activity under Visible Light. *ChemCatChem* **2013**, *5*, 2343−2351.
(22) Wang, Y.; Yao, J.; Li, H.; Su, D.; Antonietti, M. Highly Selective Hydrogenation of Phenol and Derivatives over a Pd@Carbon Nitride Catalyst in Aqueous Media. *J. Am. Chem. Soc.* **2011**, *133*, 2362−2365.
(23) Li, Y.; Xu, X.; Zhang, P.; Gong, Y.; Li, H.; Wang, Y. Highly Selective Pd@mpg-C_3N_4 Catalyst for phenol Hydrogenation in Aqueous Phase. *RSC Adv.* **2013**, *3*, 10973−10982.
(24) Li, Y.; Gong, Y.; Xu, X.; Zhang, P.; Li, H.; Wang, Y. A Practical and Benign Synthesis of Amines Through Pd@mpg-C_3N_4 Catalyzed Reduction of Nitriles. *Catal. Commun.* **2012**, *28*, 9−12.
(25) Gong, Y.; Zhang, P.; Xu, X.; Li, Y.; Li, H.; Wang, Y. A Novel Catalyst Pd@ompg-C_3N_4 for Highly Chemoselective Hydrogenation of Quinoline under Mild Conditions. *J. Catal.* **2013**, *297*, 272−280.
(26) Deng, D.; Yang, Y.; Gong, Y.; Li, Y.; Xu, X.; Wang, Y. Palladium Nanoparticles Supported on mpg-C_3N_4 as active Catalyst for Semihydrogenation of Phenylacetylene under Mild Conditions. *Green Chem.* **2013**, *15*, 2525−2531.
(27) Anderson, J. A.; Mellor, J.; Wells, R. P. K. Pd Catalysed Hexyne Hydrogenation Modified by Bi and by Pb. *J. Catal.* **2009**, *261*, 208−216.
(28) Vilé, G.; Pérez-Ramírez, J. Beyond the Use of Modifiers in Selective Alkyne Hydrogenation: Silver and Gold Nanocatalysts in Flow Mode for Sustainable Alkene Production. *Nanoscale* **2014**, *6*, 13476−13482.
(29) Wang, X.; Maeda, K.; Chen, X.; Takanabe, K.; Domen, K.; Hou, Y.; Fu, X.; Antonietti, M. *J. Am. Chem. Soc.* **2009**, *131*, 1680−1681.
(30) Lotsch, B. V. From Molecular Building Blocks to Condensed Carbon Nitride Networks: Structure and Reactivity. PhD Dissertation, LMU Munich, 2006.
(31) Zheng, Y.; Jiao, Y.; Zhu, Y.; Li, L. H.; Han, Y.; Chen, Y.; Du, A.; Jaroniec, M.; Qiao, S. Z. Hydrogen Evolution by a Metal-Free Electrocatalyst. *Nat. Commun.* **2014**, *5*, 3783.
(32) Panasiuk, Y. V.; Raevskaya, A. E.; Stroyuk, O. L.; Lytvyn, P. M.; Kuchmiy, S. Y. Preparation and Optical Properties of Highly Luminescent Colloidal Single-Layer Carbon Nitride. *RSC Adv.* **2015**, *5*, 46843−46849.
(33) Chen, Z. P.; Antonietti, M.; Dontsova, D. Enhancement of the Photocatalytic Activity of Carbon Nitrides by Complex Templating. *Chem. - Eur. J.* **2015**, *21*, 10805−10811.
(34) Shalom, M.; Inal, S.; Fettkenhauer, C.; Neher, D.; Antonietti, M. Improving Carbon Nitride Photocatalysis by Supramolecular Preorganization of Monomers. *J. Am. Chem. Soc.* **2013**, *135*, 7118−7121.
(35) Vilé, G.; Almora-Barrios, N.; Mitchell, S.; López, N.; Pérez-Ramírez, J. From the Lindlar Catalyst to Supported Ligand-Modified Palladium Nanoparticles: Selectivity Patterns and Accessibility Constraints in the Continuous-Flow Three-Phase Hydrogenation of Acetylenic Compounds. *Chem. - Eur. J.* **2014**, *20*, 5926−5937.
(36) Vilé, G.; Baudouin, D.; Remediakis, I. N.; Copéret, C.; López, N.; Pérez-Ramírez, J. Silver Nanoparticles for Olefin Production: New Insights into the Mechanistic Description of Propyne Hydrogenation. *ChemCatChem* **2013**, *5*, 3750−3759.
(37) Vilé, G.; Albani, D.; Nachtegaal, M.; Chen, Z.; Dontsova, D.; Antonietti, M.; López, N.; Pérez-Ramírez, J. A stable single-site palladium catalyst for hydrogenations. *Angew. Chem., Int. Ed.* **2015**, *54*, 11265−11269.
(38) Vilé, G.; Wrabetz, S.; Floryan, L.; Schuster, M. E.; Girgsdies, F.; Teschner, D.; Pérez-Ramírez, J. Stereo and Chemoselective Character of Supported CeO_2 Catalysts for Continuous-Flow Three-Phase Alkyne Hydrogenation. *ChemCatChem* **2014**, *6*, 1928−1934.
(39) Øygarden, A. H.; Pérez-Ramírez, J.; Waller, D.; Schöffel, K.; Brackenbury, D. Patent Appl. WO2004/110622, 2004.
(40) Schwarze, M.; Stellmach, D.; Schroder, M.; Kailasam, K.; Reske, R.; Thomas, A.; Schomacker, R. Quantification of Photocatalytic Hydrogen Evolution. *Phys. Chem. Chem. Phys.* **2013**, *15*, 3466−3472.
(41) Tarazona, P. Free-Energy Density Functional for Hard Spheres. *Phys. Rev. A: At., Mol., Opt. Phys.* **1985**, *31*, 2672−2679.
(42) Tarazona, P.; Marini Bettolo Marconi, U.; Evans, R. Phase Equilibria of Fluid Interfaces and Confined Fluids. *Mol. Phys.* **1987**, *60*, 573−595.
(43) Krumeich, F.; Mueller, E.; Wepf, R. A.; Nesper, R. Characterization of Catalysts in an Aberration-Corrected Scanning Transmission Electron Microscope. *J. Phys. Chem. C* **2011**, *115*, 1080−1083.
(44) Shirley, D. A. High-Resolution X-Ray Photoemission Spectrum of the Valence Bands of Gold. *Phys. Rev. B* **1972**, *5*, 4709−4714.
(45) Wagner, C. D.; Davis, L. E.; Zeller, M. V.; Taylor, J. A.; Raymond, R. H.; Gale, L. H. Empirical Atomic Sensitivity Factors for Quantitative Analysis by Electron Spectroscopy for Chemical Analysis. *Surf. Interface Anal.* **1981**, *3*, 211−225.
(46) Krishnan, R. Fundamentals of Semiconductor Electrochemistry and Photoelectrochemistry. In *Encyclopedia of Electrochemistry*; Bard, A. J., Stratmann, M., Licht, S., Eds.; Wiley-VCH: Weinheim, Germany, 2007; pp 1−53.

DOI: 10.1021/acsnano.5b04210
ACS Nano 2016, 10, 3166−3175